Electromechanical properties of dried tendon and iso-electrically focused collagen hydrogels

D. Denning [a,b], M. T. Abu-Rub [c], D. I. Zeugolis [c], S. Habelitz [d], A. Pandit [c], A. Fertala [e], B. J. Rodriguez [a,b*]

[a]Conway Institute of Biomolecular and Biomedical Research, University College Dublin, Belfield, Dublin 4, Ireland.
[b]School of Physics, University College Dublin, Belfield, Dublin 4, Ireland.
[c]Network of Excellence for Functional Biomaterials, National University of Ireland, Galway, Ireland.
[d]Department of Preventive and Restorative Dental Sciences, University of California, 707 Parnassus Ave., San Francisco, CA 94143-0758, USA.
[e]Department of Orthopaedic Surgery, Thomas Jefferson University, 925 Chestnut Street, Philadelphia, PA 19107, USA.

ABSTRACT

Assembling artificial collagenous tissues with structural, functional, and mechanical properties, which mimic natural tissues, is of vital importance for many tissue engineering applications. While the electromechanical properties of collagen are thought to play a role in, e.g., bone formation and remodeling, this functional property has not been adequately addressed in engineered tissues. Here, the electromechanical properties of rat tail tendon are compared with those of dried iso-electrically focused collagen hydrogels using piezoresponse force microscopy in ambient conditions. In both the natural tissue and the engineered hydrogel, D-periodic, type I collagen fibrils are observed, which exhibit shear piezoelectricity. While both tissues also exhibit fibrils with parallel orientation, Fourier transform analysis has revealed that the degree of parallel alignment of the fibrils in the tendon is three times that of the dried hydrogel. The results obtained demonstrate that iso-electrically focused collagen has similar structural and electromechanical properties to that of tendon, which is relevant for tissue engineering applications.

Keywords: piezoresponse force microscopy, atomic force microscopy, piezoelectricity, collagen, isoelectric focusing, tissue engineering.

---

[*] Correspondence: brian.rodriguez@ucd.ie

1. Introduction

Collagenous tissues comprise a major constituent of the extracellular matrix, providing structural support for cells, and performing important developmental and physiological functions [1]. The tissue-specific orientations of collagen fibrils give rise to different functional and mechanical properties [2]. Piezoelectricity is a functional property of collagen, and thus collagen will generate charge under strain (direct piezoelectric effect), and conversely, undergo a deformation in an applied electric field. The direct effect has been linked with the ability of bone to grow and remodel in response to directionally-dependent applied stress [3]. Studies of macroscopic electromechanical coupling have shown that collagenous tissues such as bone, tendon, dentin, and skin [3-6] all exhibit piezoelectricity. Fibril-forming collagens are composed of collagen molecules, which are hydrogen bond-stabilized, triple helical molecules consisting of three polypeptide chains [7]. Collagen monomers have a polar orientation directed from the amine (N)-terminal toward the carboxyl (C)-terminal. Type I collagen monomers self-assemble under appropriate conditions to form fibrils, which maintain the unipolar (N to C) orientation of the monomers at the fibril ends [2]. The staggered stacking of collagen monomers in a fibril gives rise to the characteristic 67 nm D-periodicity, which corresponds to the gap and overlap regions of the monomers, while the cross-sectional hexagonal packing of collagen molecules has been suggested as the origin of collagen piezoelectricity [5].

Previous studies have demonstrated the potential of collagenous scaffolds [8] and hydrogels [9] for tissue engineering applications [10]. The ability to assemble collagenous scaffolds *in vitro* with the same structure and properties as natural collagenous tissue would be of significant importance for studying cell-matrix interactions as well as for developing compatible engineered tissues. In addition, comparing the electromechanical properties of natural collagenous tissues and engineered collagenous constructs could help understand the biological significance of piezoelectricity in collagen. Numerous approaches to assemble fibrillar collagen structures have been implemented, including hydrodynamic flow in the presence of potassium [11, 12], magnetic field alignment [13], dip-pen lithography [14], chemical nanopatterning [15], microfluidics [16], and atomic force microscopy (AFM) manipulation [17]. Recent attempts to align collagen by electrochemical processes have demonstrated successful alignment of anisotropically-oriented collagen monomers [9, 18]. In addition to advantages such as increased mechanical stability [19], aligned collagenous tissues have been shown to influence cell alignment and growth [20].

There are several well-established methods for structural imaging of collagen fibrils and connective tissues, including scanning electron microscopy and transmission electron microscopy (TEM) [21, 22]; however, these techniques require dehydrated specimens and TEM can only provide information on polar order via staining, whilst revealing no information on electromechanical coupling. AFM allows measurements to be performed in air, liquid, and in physiologically relevant conditions, and recent advances in AFM have contributed to understanding biofunctionality at the nanoscale [23], including nanomechancial mapping of elasticity in mineralized and non-mineralized collagen fibrils [24–26]. Piezoresponse force microscopy (PFM), a technique developed initially to image domains in ferroelectric materials by measuring bias-induced surface deformations [27], has recently been employed to study electromechanical coupling in biological systems [28]. PFM is capable of investigating in-plane and out-of-plane piezoelectric response from biosystems at the nanoscale, including collagen [29–33]. Minary-Jolandan and Yu have observed shear piezoelectricity in single collagen type I fibrils using PFM [31, 32]. With PFM, not only can fibril alignment be investigated through normal AFM surface topography and deflection images, but the amplitude of the piezoelectric signal and the polarity of the fibrils can be imaged.

Cells have been shown to co-align with aligned collagen fibrils, suggesting that ordered fibrils influence cell polarization [34]. It has also been shown that cells align in the direction of mechanical loading in hydrogels [35], which has been attributed to the triggering of cell-surface stretch receptors by mechanical signals. It seems plausible to suggest that such mechanical signals could transform into electrical signals as a result of collagen piezoelectricity. Previous studies have also shown that electrical signals of various strengths and pulses lead to a significant increase in bone cell proliferation [36].

Successfully assembling collagen-rich tissues with similar alignment, orientation, and piezoelectric properties as natural tissues will provide a framework to further our understanding of the role collagen structure and function has on intercellular and cell-matrix communication. The ability to study the piezoelectricity of collagen on the nanoscale will provide a pathway towards understanding mechanotransduction mechanisms and the role electromechanics plays in bone remodeling and tissue growth. There may be unidentified benefits of replicating both *functional* and *structural* properties of collagenous tissues. By replicating the phenomenon of electromechanical coupling in assembled tissues, the applications of engineered collagen structures can be expanded. Notably, electromechanical coupling is a phenomenon exhibited by many biopolymers [3], including chitin, cellulose, poly-L-lysine, etc., which are currently used for biomedical applications [37]. Piezoelectric polymers have also been shown to promote neurite alignment [38]. It is envisioned that not just the structural and chemical properties of such biomaterials should be tailored, but so should the electromechanical properties, in order to elicit desired outcomes for targeted applications.

Here, a comparison of the electromechanical properties of iso-electrically focused collagen with rat tail tendon is presented. Rat tail tendon is an excellent tissue for studying collagen as it consists primarily of type I collagen, with only a small volume of proteoglycan, in which the fibrils have a high degree of alignment along the tendon axis [39]. Similarly, iso-electric focusing has been shown induce the conformational alignment of collagen monomers, which then assemble into hierarchical structures (nano- and micro-fibrils) that co-align along axis of the hydrogels [9].

2. Materials and Methods

2.1 Preparation of rat tail tendon

Tendon harvested from a rat tail has been deposited on gold-coated mica, fixed via carbon tape, and allowed to dry. The tendon fiber used for the study is 440 ± 20 μm in diameter and 4.2 ± 0.02 mm in length, measured via a micrometer. The tendon has been bleached in a 4% sodium hypochlorite solution for 20 s in order to partially remove non-collagenous proteins, and thereby expose the fibrils.

2.2 Preparation of iso-electrically focused collagen

Self-assembled, iso-electrically focused collagen hydrogels have been prepared via a method described previously by Abu-Rub *et al.* [9]. Briefly, a solution of dialyzed type I collagen monomers in a 20 nM acetic acid solution is subjected to a DC voltage of 3 V at a current of 25 μA in an electrochemical cell for 60 min. This generates a pH gradient between the electrodes, which causes the collagen monomers to migrate towards their isoelectric point (pH of 8). The monomers concentrate and subsequently assemble along this region to form a dense fiber bundle, which is then removed and incubated in polyethylene glycol (PEG)-containing buffer at 37 °C prior to incubation in phosphate buffered saline (PBS) overnight. The collagen hydrogel is then placed on highly ordered pyrolytic graphite and allowed to dry in air prior to PFM measurements. The dried collagen hydrogel used in the study is 500 ± 20 μm in diameter and 6.50 ± 0.02 mm in length.

2.3 Atomic force microscopy and piezoresponse force microscopy experiments

PFM imaging has been performed with an Asylum Research MFP-3D AFM equipped with a Zurich Instruments HF2LI lock-in amplifier and using conductive MikroMasch DPE18 Pt-coated cantilevers with nominal resonant frequencies and spring constants of 75 kHz and 3.5 N/m, respectively. The cantilever stiffness is expected to minimize any electrostatic contribution to the measured signal [40]. Prior to imaging, the rat tail tendon and iso-electrically focused collagen samples are placed on a grounded copper plate. During imaging, an AC signal, $A_0 \sin(\omega t)$ (typically 30 V_{rms} at 7 kHz), is applied to the tip, which is in contact with the surface at a constant force (typically 90 nN). The resulting local shear deformations are detected via photodetector signal changes due to cantilever torsion. In this scenario, the in-plane polarization is measured, and the technique is typically referred to as lateral PFM (LPFM) [41]. The shear sensitivity was calculated based on the geometry of the cantilever, as described by Peter *et al.* [42], using the equation, $R=4L/3h$, where R is the ratio between the in-plane and out-of-plane sensitivities, L is the length of the cantilever (230 μm), and h is the combined height of the tip and cantilever thickness (18 μm). The out-of-plane sensitivity was experimentally measured (53.6 nm/V), therefore the in-plane sensitivity is 913 nm/V.

The orientation of collagen fibrils, which exhibit shear piezoelectricity, with respect to the cantilever axis can affect the magnitude of the piezoelectric signal obtained. Thus, the sensitivity of the piezoresponse due to fibril-cantilever geometries must be considered. The maximum detected shear piezoelectric deformation of a single collagen fibril on a substrate due to an applied field occurs when the cantilever axis is perpendicular to the fibril polarization [43]. This geometry also minimizes any contribution of cantilever buckling with the measured lateral signal. High voltage PFM has been implemented using a custom-built amplifier based on an APEX model PA85 operational amplifier with a gain of 10, which amplified the AC excitation signal. The piezoelectric signal, $A_1 \sin(\omega t + \Phi)$, resulting from the converse piezoelectric effect and measured via the torsion of the cantilever, is demodulated into amplitude (A_1) and phase (Φ) signals using the lock-in amplifier. The acquired PFM amplitude and phase response images indicate the amplitude of the piezoelectric shear deformation and the N to C polarity of the collagen, respectively.

Fibril widths have been estimated from the AFM line profiles of ten fibrils. AFM deflection images are used as individual fibrils are visible in both the dried hydrogel and tendon in these images. For each fibril width reported, three line profiles are taken along the length of the fibril to account for any non-uniform fibrillar widths. Only fibrils which were visibly isolated were chosen for analysis.

2.4 Fast Fourier transform analysis

Fast Fourier transform (FFT) analysis (WSxM [44]) has been used to characterize the alignment of collagen fibrils from both rat tail tendon and iso-electrically focused collagen. By conducting FFT analysis on an image, the information in the image is converted into frequency space. The subsequent FFT output image contains pixels which are distributed in a shape which represents the degree of alignment in the original image. In general, the more symmetric the shape is, the higher the degree of alignment which is present in the image. Direct comparison of the FFTs from rat tendon and the dried collagen hydrogel is possible using a radial profile plug-in (ImageJ). By summing the pixel intensities along the radius of the circular projection between 0° and 360° in 1° increments, the FFT distributions can be visualized and analyzed quantitatively.

3. Results and Discussion

3.1 AFM characterization of rat tail tendon and iso-electrically focused collagen hydrogel

Surface properties of rat tail tendon have been characterized via AFM. An AFM deflection image of a 5 x 5 μm^2 area of the tendon is shown in Fig. 1a. A periodic banding of 67 ± 3 nm is observed, as shown in Fig. 1c, which has been determined by measuring a line profile from ten fibrils in the image and calculating the average and standard deviation. This periodicity is more readily apparent in the deflection as opposed to height images. The fibrils appear to be predominately oriented along the long axis of the tendon. The average observed fibril width has been determined to be 232 ± 35 nm, again calculated from an average of ten fibrils in the image, which is within the range reported for rat tail tendon (typical fibril diameters are between 50 nm and 300 nm and vary with the age of the rat [39]).

Fig. 1b shows an AFM deflection image of the dried collagen hydrogel. Several fibrils are aligned along the length of the hydrogel axis, but a considerable number of misaligned fibrils remain. The line profile in Fig. 1d shows the periodic 67 ± 2 nm banding of collagen and a typical fibril width of 227 ± 46 nm. These results demonstrate the successful replication of fibrillar type I collagen with similar fibril widths. However, from this image, we see this particular collagen hydrogel does not have the same degree of fibrillar alignment as the rat tail tendon. Note that the PEG buffer stimulates volume reduction by dehydration, which assists with the fibrillar alignment, thus the tendon and hydrogel samples likely have different water contents and may deform differently during sample preparation.

3.2 PFM characterization of rat tail tendon and iso-electrically focused collagen hydrogel

As collagen is a shear piezoelectric biopolymer [5, 29], LPFM has been applied to investigate the in-plane piezoelectric response of the tendon and dried hydrogel. A 20 x 20 μm^2 area deflection image of the rat tail tendon is shown in Fig. 2a. At this scan size, there is no periodic banding visible. Note that in some regions, the tendon may not have been bleached sufficiently to reveal the fibrils. PFM, however, probes a finite volume beneath the tip such that the response of the fibrils underneath can still be visualized [45]. Fig. 2b is the corresponding LPFM amplitude image, which confirms piezoelectricity in the tendon. Each fibril appears to have a constant piezoresponse value along the length of the fibril, and the image illustrates a high degree of alignment of the fibrils. The LPFM phase image (Fig. 2c) displays the N to C polarity, or the polar order, of the collagen fibrils. Since it is non-trivial to identify the polarization direction, a fibril with bright phase contrast (+90°) is assigned as having a N to C polarity pointing to the right of the image, while a fibril with dark phase contrast (-90°) has a polar order pointing to the left. In essence, the fibrils are deforming out of phase with each other during the application of the AC bias. Note that there is clear evidence of anti-parallel polar ordering of the fibrils, whereby adjacent fibrils exhibit polarization in opposite directions. Fig. 2, d-f shows LPFM images obtained from a smaller area (5 x 5 μm^2 scan). Collagen fibrils are visible in the deflection image (Fig. 2d), as confirmed by the presence of D-periodicity. The LPFM amplitude image (Fig. 2e) displays fibrillar-level response consistent with the shear piezoelectricity of type I collagen. The average width of the fibrils in the LPFM amplitude image is 200 ± 78 nm. This suggests the response is due to the piezoelectric activity of individual fibrils as the average fibrillar widths from the AFM deflection image have been measured to be 232 ± 35 nm. From the LPFM phase image (Fig. 2f), there is further evidence of anti-parallel fibrillar ordering along the tendon axis. By comparing the LPFM phase and amplitude images, it can be observed that fibrils which exhibit opposite polarization directions undergo equal shear piezoelectric deformations, as expected.

Lateral PFM has been utilized to study electromechanical coupling in dried iso-electrically focused collagen hydrogels to compare the shear piezoelectricity of natural and engineered collagen. Fig. 3 shows the LPFM results from the iso-electric collagen. Fibrils are visible throughout the entire deflection image in Fig. 3a. From the LPFM amplitude image in Fig. 3b, piezoelectricity is confirmed in the dried hydrogel, suggesting a successful replication of this functional property. In the LPFM amplitude image, higher piezoresponse is observed from fibrils perpendicular to the cantilever and parallel to the scanning direction, which is due to the in-plane shear response of the fibrils and results from the torsional twisting of the cantilever. The cantilever-fibril geometry used for all PFM measurements is illustrated in the insets of Figs. 2a and 3a. The long axis of the tendon and dried hydrogel sample is parallel to the scanning direction in all cases. The signal dependence on the angle between the cantilever and fibril is highlighted in Fig. 3 *E*. Fibril 1 has the optimal orientation for measuring the shear response of the fibrils as it is perpendicular to the cantilever and parallel to the scan direction. Fibril 2 displays approximately half of the maximal response as it has a 37° angle with respect to the scan direction. LPFM amplitude images for rat tail tendon and the dried collagen hydrogel have been normalized to allow for direct comparison of both. From the calculated average piezoresponse from the amplitude images measured on both samples, the collagen hydrogel has a 35% higher signal than the tendon. There is also a higher response from fibrils with optimal orientation (perpendicular to the cantilever) in the dried collagen hydrogel when compared to similar fibrils in the rat tail tendon. This unexpected result may be attributed to incomplete bleaching (Fig. 1a) of the tendon sample or to a change in the tip state, i.e., contamination or coating wear. However, it should also be noted that while the tendon collagen fibrils are cross-linked, there is no specific cross-linking step in the preparation of the hydrogel (noncovalent cross-links are likely present in the hydrogel). This would likely result in a larger piezoelectric signal due to a higher degree of freedom of the monomers, but would require an additional study. The LPFM phase image shown in Fig. 3c displays the polar order of the fibrils where a +90° phase is observed for 81% of the image, illustrating that the anti-parallel polar ordering observed in the tendon is not replicated in the dried hydrogel.

3.3 Alignment studies of rat tail tendon and iso-electrically focused collagen hydrogel via FFT analysis

In Fig. 4, the degree of alignment of the fibrils in the tendon is investigated. The fibrillar alignment in tendon and iso-electrically focused collagen has been determined using FFT analysis of the PFM amplitude images and subsequent radial summation of pixel intensities. PFM amplitude images were chosen for the FFT analysis (as opposed to topography images) as the collagen fibrils are not fully exposed in the rat tendon case. FFT and radial averaging analysis of the phase and reconstructed A_1 sin ($\omega t + \Phi$) images follow the same trend demonstrated with the amplitude images. The FFT of an image containing aligned fibrils will yield an elliptical distribution. The degree of alignment is represented by the full width at half maximum (FWHM) of the peaks obtained from summing the pixel intensities of the FFT image for each degree between 0° and 360°. Fig. 4a shows the FFT of Fig. 2b, which has a narrow peak illustrating the alignment of the collagen fibrils in rat tail tendon. The radial summation of the intensity of the rat tail tendon FFT image (Fig. 4c) reveals two peaks at 95° and 275°, indicating strong alignment along the scan direction, and hence, along the tendon axis. The slight offset from 90° and 270° is due to a slight misalignment of the scan direction with respect to the tendon axis. The FWHM of the peaks has been determined to be 34° and 42°, respectively. The radially-averaged intensity plots have been normalized using a scaling factor of 3300 to allow for direct comparison between tissues.

The alignment of collagen fibrils in the dried iso-electrically focused collagen hydrogel has also been studied using FFT analysis (Fig. 4b). From the radial summation of the FFT image (Fig. 4c), there are peaks at 85° and 275°, and the FWHM is measured to be 95° and 135°, respectively. Comparing the average FWHM value for the tendon and dried hydrogel (38° and 115°, respectively), it is apparent that the collagen fibrils in the tendon are three times as well-aligned as those in the hydrogel.

4. Conclusion

Piezoresponse force microscopy measurements have been performed on both collagen from rat tail tendon and a dried collagen hydrogel formed by iso-electric focusing to study the alignment of both tissues and to investigate their electromechanical properties. In the tendon sample, collagen fibrils display a high degree of alignment, which is always observed along the length of the long axis of the tendon. LPFM results confirm shear, fibrillar-level piezoelectricity in the tendon, and strong evidence of anti-parallel polar ordering of neighboring fibrils in rat tail tendon is observed in both large (20 μm) and small (5 μm) scale PFM images. It has been shown that the dried collagen hydrogel successfully replicates the characteristic D-period of natural type I fibrillar collagen in tendon. PFM images measured on the dried collagen hydrogel verify the piezoelectricity of the engineered tissue, demonstrating that iso-electrically focused collagen has similar piezoelectric properties as natural collagen in tendon. The higher piezoresponse signal observed in the dried hydrogel is thought to result from the lack of covalent crosslinks present in the engineered tissue. More study is required on the role of covalent crosslinks on the piezoelectricity of biosystems. The work presented here has implications for exploiting piezoelectric biopolymers in tissue engineering applications, which may further our understanding of the role of collagen structure and function on intercellular and cell-matrix communication.

Acknowledgements

This publication has emanated from research conducted with the financial support of Science Foundation Ireland under grant numbers (SFI10/RFP/MTR2855 and SFI07/SRC/B1163). The authors are grateful for the support of the Nanoscale Function Group and in particular J.I. Kilpatrick and S.H. Loh for building the high voltage amplifier used in this study, and L. Collins and S.A.L. Weber for technical assistance and insightful discussions.

References

1. Fratzl P. Collagen: Structure and Mechanics. Springer Science+Business Media: New York; 2008.
2. Prockop DJ, Fertala A. The collagen fibril: the almost crystalline structure. J Struct Bio 1998;122:111–118.
3. Fukada E. History and recent progress in piezoelectric polymers. UFFC IEEE Trans 2000;47:1277–1290.
4. Marino AA, Becker RO. Piezoelectric effect and growth control in bone. Nature 1970;228:473–474.
5. Fukada E, Yasuda I. On the piezoelectric effect of bone. J Phys Soc Japan 1957;12:1158–1162.
6. Marino AA, Gross BD. Piezoelectricity in cementum, dentine and bone. Arch Oral Biol 1989;34:507–509.
7. Wess T, Hammersley A, Wess L, Miller A. Molecular packing of type I collagen in tendon. J Molec Bio 1998;275:255–267.
8. Torbet J et al. Orthogonal scaffold of magnetically aligned collagen lamellae for corneal stroma reconstruction. Biomaterials 2007;28:4268–4276.
9. Abu-Rub MT et al. Nano-textured self-assembled aligned collagen hydrogels promote directional neurite guidance and overcome inhibition by myelin associated glycoprotein. Soft Matter 2011;7:2770–2781.
10. Kato YP, Christiansen DL, Hahn RA, Shieh SJ, Goldstein JD, Silver FH. Mechanical properties of collagen fibres: a comparison of reconstituted and rat tail tendon fibres. Biomaterials 1989;10:38–42.
11. Jiang F, Horber H, Howard J, Muller DJ. Assembly of collagen into microribbons: effects of pH and electrolytes. J Struc Bio 2004;148:268–278.
12. Loo RW, Goh MC. Potassium ion mediated collagen microfibril assembly on mica. Langmuir 2008;24:13276–13278.
13. Torbet J, Ronzière MC. Magnetic alignment of collagen during self-assembly. Biochem J 1984;219:1057–1059.
14. Wilson DL, Martin R, Hong S, Cronin-Golomb M, Mirkin CA, Kaplan DL. Surface organization and nanopatterning of collagen by dip-pen nanolithography. Proc Natl Acad Sci USA 2001;98:13660–13664.
15. Denis FA, Pallandre A, Nysten B, Jonas AM, Dupont Gillain CC. Alignment and assembly of adsorbed collagen molecules induced by anisotropic chemical nanopatterns. Small 2005;1:984–991.
16. Lee P, Lin R, Moon J, Lee LP. Microfluidic alignment of collagen fibers for in vitro cell culture. Biomed Microdev 2006;8:35–41.
17. Jiang F, Khairy K, Poole K, Howard J, Müller DJ. Creating nanoscopic collagen matrices using atomic force microscopy. Microsc Res Techniq 2004;64:435–440.
18. Cheng X, Gurkan UA, Dehen CJ, Tate MP, Hillhouse HW, Simpson GJ, Akkus O. An electrochemical fabrication process for the assembly of anisotropically oriented collagen bundles. Biomaterials 2008;29:3278–3288.
19. Pins GD, Christiansen DL, Patel R, Silver FH. Self-assembly of collagen fibers. Influence of fibrillar alignment and decorin on mechanical properties. Biophys J 1997;73:2164–2172.

20. Murugan R, Ramakrishna S. Design strategies of tissue engineering scaffolds with controlled fiber orientation. Tissue Eng 2007;13:1845–1866.
21. Birk DE, Hahn RA, Linsenmayer CY, Zycband EI. Characterization of collagen fibril segments from chicken embryo cornea, dermis and tendon. Matrix Biol 1996;15:111–118.
22. Birk DE, Trelstad RL. Extracellular compartments in tendon morphogenesis: collagen fibril, bundle, and macroaggregate formation. J Cell Bio 1986;103:231–240.
23. Hansma HG, Hoh JH. Biomolecular imaging with the atomic force microscope. Annu Rev Biophys Biomol Struc 1994;23:115–140.
24. Wenger MPE, Bozec L, Horton MA, Mesquida P. Mechanical properties of collagen fibrils. Biophys J 2007;93:155.1263.
25. Balooch M, Habelitz S, Kinney JH, Marshall SJ, Marshall GW. Mechanical properties of mineralized collagen fibrils as influenced by deminerlization. J Struct Bio 2008;162:404–410.
26. Minary-Jolandan M, Yu MF. Nanomechanical heterogeneity in the gap and overlap regions of type I collagen fibrils with implications for bone heterogeneity. Biomacromolecules 2009;10:2565–2570.
27. Gruverman A, Auciello O, Tokumoto H. Imaging and control of domain structures in ferroelectric thin films via scanning force microscopy. Annu Rev Mater Sci 1998;28:101–123.
28. Kalinin SV, Rodriguez BJ, Jesse S, Karapetian E, Mirman B, Eliseev EA, Morozovska AN. Nanoscale electromechanics of ferroelectric and biological systems: A new dimension in scanning probe microscopy. Annu Rev Mater Res 2007;37:189–238.
29. Halperin C, Mutchnik S, Agronin A, Molotskii M, Urenski P, Salai M, Rosenman G. Piezoelectric Effect in Human Bones Studied in Nanometer Scale. Nano Letters 2004;4:1253–1256.
30. Rodriguez BJ et al. Electromechanical imaging of biomaterials by scanning probe microscopy. J Struc Bio 2006;153:151–159.
31. Minary-Jolandan M, Yu MF. Nanoscale characterization of isolated individual type I collagen fibrils: polarization and piezoelectricity. Nanotechnology 2009;20:085706.
32. Minary-Jolandan M, Yu MF. Uncovering nanoscale electromechanical heterogeneity in the subfibrillar structure of collagen fibrils responsible for the piezoelectricity of bone. ACS Nano 2009;3:1859–1863.
33. Harnagea C et al. Two-dimensional nanoscale structural and functional imaging in individual collagen type I fibrils. Biophys J 2010;98:3070–3077.
34. Friedrichs, J, Taubenberger A, Franz CM, Muller DJ. Cellular remodelling of individual collagen fibrils visualized by time-lapse AFM. J Mol Bio 2007;372:594–607.
35. Altman G et al. Cell differentiation by mechanical stress. FASEB J 2002;16:270–272.
36. Brighton CT, Okereke E, Pollack SR, Clark CC. In vitro bone-cell response to a capacitively coupled electrical field The role of field strength, pulse pattern, and duty cycle. Clin Orthop Relat Res 1992; 285:255–262.
37. Nair LS, Laurencin CT. Biodegradable polymers as biomaterials. Prog Polym Sci 2007;32:762-798.
38. Lee Y, Collins G, Arinzeh TL. Neurite extension of primary neurons on electrospun piezoelectric scaffolds. Acta Biomater 2011;7:3877–3886.

39. Scott JE, Orford CR, Hughes EW. Proteoglycan-collagen arrangements in developing rat tail tendon. An electron microscopical and biochemical investigation. Biochem J 1981;195:573–581.
40. Christman JA, Woolcott RR Jr, Kingon AI, Nemanich RJ. Piezoelectric measurements with atomic force microscopy. App Phys Lett 1998;73:3851–3853.
41. Abplanalp M, Eng, LM, Günter P. Mapping the domain distribution at ferroelectric surfaces by scanning force mircoscopy. Appl Phys A 1998;66:231–234.
42. Peter F, Rüdiger A, Waser R, Szot K, Reichenberg B. Comparison of in-plane and out-of-plane optical amplification in AFM measurements. Rev Sci Instrum 2005;76:046101.
43. Sharma P, Wu D, Poddar S, Reece TJ, Ducharme S, Gruverman A. Orientational imaging in polar polymers by piezoresponse force microscopy. J Appl Phys 2011;110:052010.
44. Horcas I, Fernández R, Gómez-Rodríguez JM, Colchero J, Gómez-Herrero J, Baro AM. WSXM: A software for scanning probe microscopy and a tool for nanotechnology. Rev Sci Instrum 2007;78:013705.
45. Kalinin SV, Karapetian E, Kachanov M. Nanoelectromechanics of piezoresponse force microscopy. Phys Rev B 2004;70:184101.

Figure Captions

Fig. 1. AFM images of rat tail tendon and iso-electrically focused hydrogel. (a) AFM deflection image of a rat tail tendon. (b) AFM deflection image of iso-electrically focused collagen. (c) Line profile measured from (a) displaying the periodicity of the collagen fibrils. (d) Line profile measured from (b) confirming collagen periodicity in iso-electrically focused collagen fibrils. Scale bar for (a) and (b) is 1 μm.

Fig. 2. PFM images of rat tail tendon. (a) AFM deflection image of a rat tail tendon. The inset shows the cantilever orientation and scanning direction (double arrow). (b) LPFM amplitude image measured in the same region as (a). (c) LPFM phase image displaying the polar orientation of the fibrils. Scale bar for (a–c) is 5 μm. (d) Smaller scan size AFM image measured from the location indicated by the square in (b), which shows the periodicity of the fibrils. (e) LPFM amplitude and (f) LPFM phase images of the same region as (d). Arrows in (f) indicate the assigned collagen polarity from N to C termini. Scale bar for (d–f) is 1 μm.

Fig. 3. PFM images of iso-electrically focused collagen hydrogel. (a) AFM deflection image of iso-electrically focused collagen. The inset shows the cantilever orientation and scanning direction (double arrow). (b) LPFM amplitude image of same area as (a) and simultaneously recorded (c) LPFM phase image. Scale bar for (a–c) is 5 μm. (d) Smaller scan size AFM deflection image of iso-electrically focused collagen measured from the location indicated by the square in (b). (e) LPFM amplitude and (f) LPFM phase images. The regions circled in (e) show (1) a fibril aligned with the scan direction, and (2) a fibril oriented at an angle with respect to the scan direction. Arrows in (f) indicate the assigned collagen polarity from N to C termini. Scale bar for (d–f) is 1 μm.

Fig. 4. FFT analysis of rat tail tendon and iso-electrically focused hydrogel. (a) FFT of the rat tail tendon PFM amplitude image (Fig. 2b) displaying the fibrillar alignment of natural tissue. (b) FFT of the iso-electrically focused collagen PFM amplitude image (Fig. 3b) displaying alignment of grown fibrils. (c) Radial average intensity plot of the rat tail tendon FFT and iso-electrically focused FFT images.

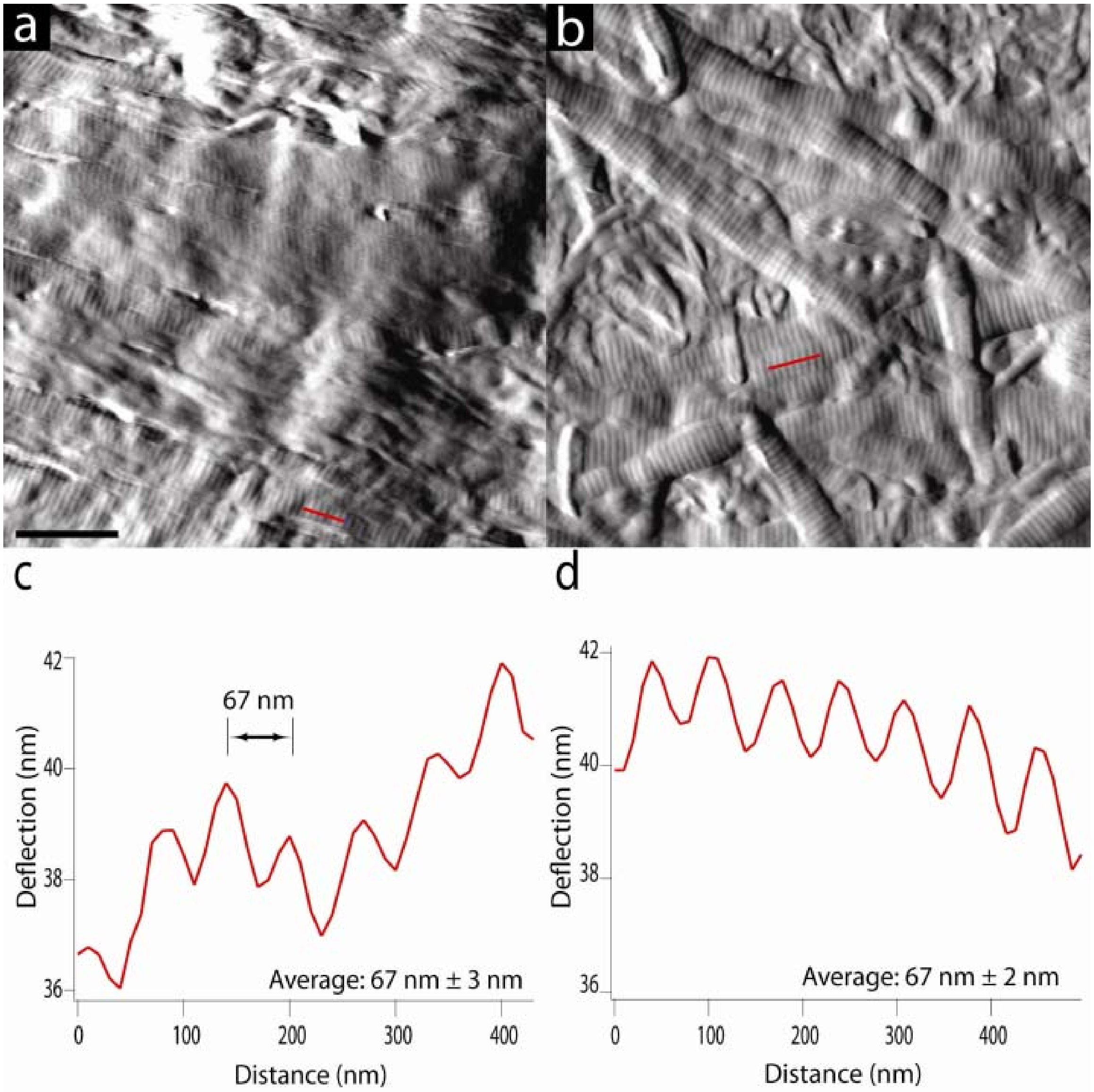

D. Denning *et al*., Figure 1

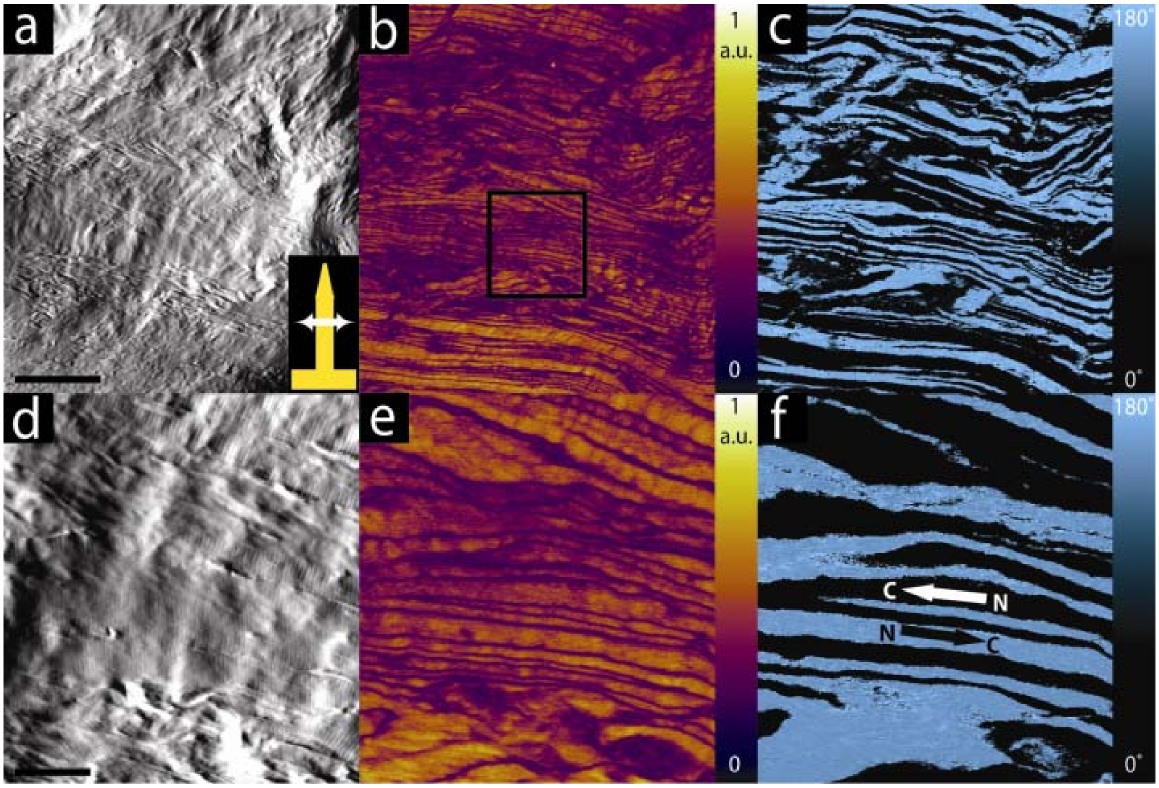
a
b
1
a.u.
0
c
180°
0°
d
e
1
a.u.
0
f
180°
0°
C
N
N
C

D. Denning *et al*., Figure 2

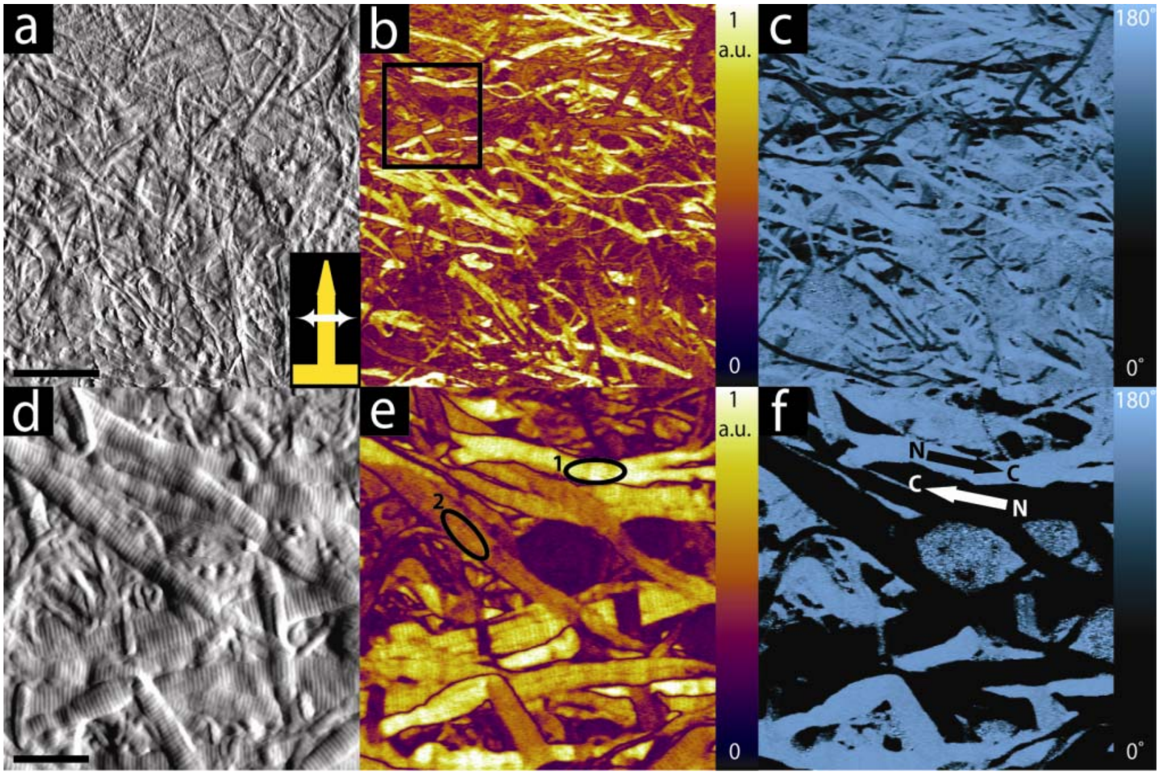
a
b
1
a.u.
0
c
180°
0°
d
e
1
a.u.
0
1
2
f
180°
0°
N
C
C
N

D. Denning *et al*., Figure 3

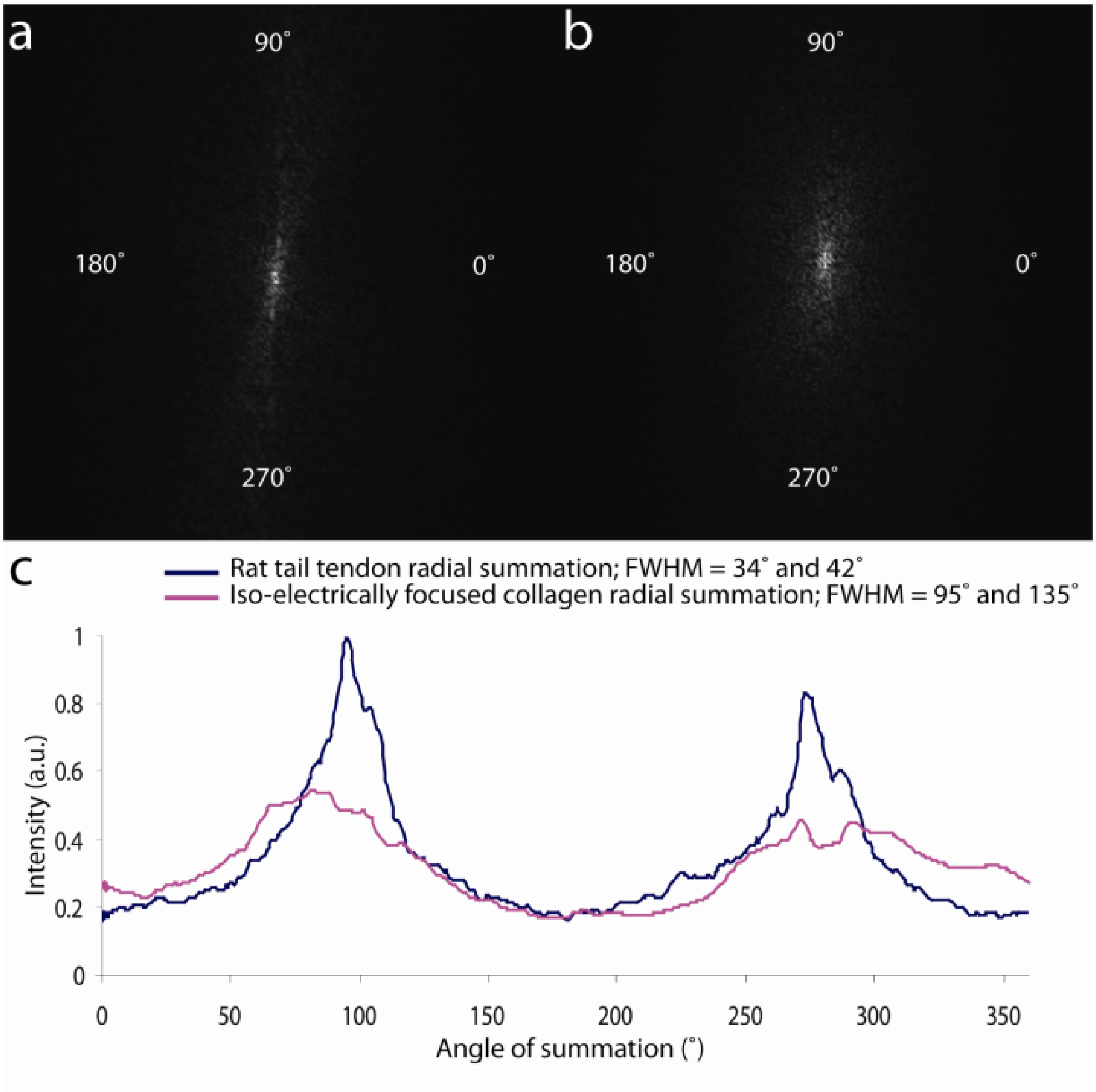

D. Denning *et al*., Figure 4